Near-field radiative heat transfer between chiral metamaterials

Cite as: J. Appl. Phys. **112**, 084309 (2012); https://doi.org/10.1063/1.4759055
Submitted: 21 June 2012 . Accepted: 19 September 2012 . Published Online: 18 October 2012

Longji Cui, Yong Huang, and Ju Wang

Near-field radiative heat transfer between chiral metamaterials

Longji Cui, Yong Huang,[a] and Ju Wang
Fundamental Science on Ergonomics and Environment Control Laboratory, School of Aeronautic Science and Engineering, Beihang University, Beijing 100191, China

(Received 21 June 2012; accepted 19 September 2012; published online 18 October 2012)

We investigate the near-field radiative heat transfer between two dispersive and lossy chiral metamaterials. Our theory takes into account the magnetoelectric coupling effect compared with the existing theories. It is shown that the contribution of surface modes to heat transfer is strongly modulated by the magnetoelectric coupling effect. We predict that in the presence of strong coupling effect, the resonant tunneling modes with small parallel wavenumbers activate a novel energy transfer channel. We also find that the dissipation effect in material, which is characterized by the scattering rate, significantly influences the effect of magnetoelectric coupling on near-field heat transfer. We finally discuss the applications of these results in thermophotovoltaic energy conversion and the experimental realization of near-field heat transfer. © *2012 American Institute of Physics*. [http://dx.doi.org/10.1063/1.4759055]

I. INTRODUCTION

Radiative heat exchange between two objects can excess the blackbody radiation limit, when separation distance is less than the characteristic thermal wavelength. Such enhancement is due to photon tunneling of evanescent waves in the near-field regime.[1–3] Based on fluctuational electrodynamics introduced by Rytov,[4] extensive researches investigate near-field heat transfer in various geometrical configurations[5–13] and for different material properties.[14–18] In particular, it has been demonstrated[1] that the near-field heat transfer can be several orders of magnitude larger than the blackbody radiation, if thermal excited surface modes (i.e., surface polaritons SPs) mediate in the transfer. Recent experiments[19–21] have quantitatively confirmed the near-field effects between dielectrics in the configurations of microsphere-plane and two parallel planes. Near-field heat transfer has opened new possibilities for numerous promising applications, such as imaging,[22] thermal rectification,[23] nano-thermal patterning,[24] and energy conversion.[25]

Recently, the theory of near-field heat transfer has also been applied to metamaterials.[26–28] These materials are built with artificial resonators that can produce desired electromagnetic responses and provide flexibility in manipulating electromagnetic waves. It is shown that two closely spaced metamaterials can further increase the radiative heat transfer due to novel heat flux channel activated by magnetic surface modes.[26] On the other hand, a new class of metamaterial, chiral metamaterials (CMMs), has recently attracted much attention. In ordinary metamaterials, electric and magnetic responses are produced by two sets of resonators.[29] In contrast, in CMMs there exists a cross-coupled electromagnetic response obtained by a chiral resonator.[30] This magnetoelectric coupling effect was first proposed as an alternative methodology to achieve negative refraction.[30–32] In terms of light-matter interactions, this property indicates an extra degree of freedom in controlling electromagnetic waves and might bring new applications that go beyond ordinary metamaterials. Despite the progress in the field of near-field radiative heat transfer, a still open question is how energy is exchanged in the presence of magnetoelectric coupling effect.

In this paper, we investigate the near-field heat transfer between two CMMs using the fluctuational electrodynamics. It is shown that the SPs mediated radiative transfer can be further modulated by magnetoelectric coupling effect, and a novel heat energy transfer channel is activated in the presence of strong coupling effect.

II. NEAR-FIELD RADIATIVE HEAT TRANSFER BETWEEN TWO CHIRAL MEDIA

Consider chiral media 1 and 2 occupying the half-space $z<0$ and $z>d$, and separated by a vacuum gap. Assume both media are in local thermodynamic equilibrium, with temperature T_1 and T_2, respectively. The spectral radiative heat transfer between two objects is equal to the normal component of the ensemble averaged Poynting vector[33]

$$S_\omega = 2\mathrm{Re}\langle \mathbf{E}(r,\omega) \times \mathbf{H}^\dagger(r,\omega)\rangle, \tag{1}$$

where $\mathbf{E}(r,\omega)$ and $\mathbf{H}^\dagger(r,\omega)$ are the Fourier component of fluctuation electric and conjugated magnetic field at position r. The electromagnetic field can be solved by the fluctuation Maxwell equations as well as the constitute relation, which for chiral media is[34]

$$\begin{aligned} \mathbf{D} &= \varepsilon_0\varepsilon\mathbf{E} + i\frac{\kappa}{c}\mathbf{H}, \\ \mathbf{B} &= \mu_0\mu\mathbf{H} - i\frac{\kappa}{c}\mathbf{E}, \end{aligned} \tag{2}$$

where $\varepsilon_0(\mu_0)$ are permittivity (permeability) in vacuum, ε and μ are relative permittivity and permeability, respectively, κ is the chirality parameter, and c is the light speed. For

[a]Electronic mail: huangy_zl@263.net.

mathematical convenience, another choice of constitutive relation is written in the Drude-Born-Fedorov type

$$\begin{aligned}\mathbf{D} &= \varepsilon_0\varepsilon_{DBF}(\mathbf{E} + \beta\nabla \times \mathbf{E}),\\ \mathbf{B} &= \mu_0\mu_{DBF}(\mathbf{H} + \beta\nabla \times \mathbf{H}),\end{aligned} \tag{3}$$

where β, ε_{DBF}, and μ_{DBF} are chirality, permittivity, and permeability, respectively. Though Eqs. (2) and (3) are written in different forms, they are indeed equivalent descriptions, and the corresponding parameters are linked by some algebraic transformations. Define a dielectric tensor from Eq. (3) as $\tilde{\varepsilon} = \varepsilon_{DBF} + \varepsilon_{DBF}\beta[\nabla]$ and a magnetic tensor as $\tilde{\mu} = \mu_{DBF} + \mu_{DBF}\beta[\nabla]$, where $[\nabla]$ denotes the cross-product operation. Thus, we get a constitutive relation sharing the similar form with isotropic and anisotropic materials

$$\mathbf{D} = \varepsilon_0\tilde{\varepsilon}\mathbf{E}, \quad \mathbf{B} = \mu_0\tilde{\mu}\,\mathbf{H}. \tag{4}$$

Given the constitutive relation, radiative heat transfer in a certain geometrical configuration can be evaluated by determining the electric Green's dyadic $\mathbf{G}(\mathbf{r}, \mathbf{r}')$ with $\mathbf{r}$ and $\mathbf{r}'$ in the vacuum gap, which obeys the monochromatic equation[35]

$$\left(\nabla \times \frac{1}{\mu_0}\nabla \times -\varepsilon_0\frac{\omega^2}{c^2}\right)\mathbf{G}(\mathbf{r}, \mathbf{r}', \omega) = \mathbf{I}\delta(r - r'). \tag{5}$$

Note that the physical meaning of Eq. (5) is apparent if we consider a dipole placed within the vacuum gap oscillating and generating electromagnetic waves with total vector potential $\mathbf{G}(\mathbf{r}, \mathbf{r}', \omega)$. Thus, it is clear that $\mathbf{G}(\mathbf{r}, \mathbf{r}', \omega)$ contains all waves confined between the surfaces and undergoing multiple reflections (MRs) within the gap. The final form of $\mathbf{G}(\mathbf{r}, \mathbf{r}', \omega)$ is obtained by summing up the contributions of all waves[18]

$$\mathbf{G} = \frac{i}{2\gamma}(\mathbf{D}_{12}e^{i\gamma z} + \mathbf{D}_{21}\mathbf{R}_2e^{2i\gamma d}e^{-i\gamma z})(\mathbf{I}e^{-i\gamma z'} + \mathbf{R}_1e^{i\gamma z'}), \tag{6}$$

where $\gamma = \sqrt{k_0^2 - \mathrm{k}_{||}^2}$ is the normal component of the wave vector, with $k_0 = \omega/c$ and $\mathrm{k}_{||}$ the parallel components of the wave vector, $\mathbf{D}_{12} = (\mathbf{I} - \mathbf{R}_1\mathbf{R}_2\mathrm{e}^{-2|\gamma|d})^{-1}$ is a geometric series accounting for the MRs of waves, and $\mathbf{R}_i$ is the matrix of reflection coefficients

$$\mathbf{R}_i = \begin{bmatrix} r_i^{ss}(\omega, \mathrm{k}_{||}) & r_i^{sp}(\omega, \mathrm{k}_{||}) \\ r_i^{ps}(\omega, \mathrm{k}_{||}) & r_i^{pp}(\omega, \mathrm{k}_{||}) \end{bmatrix}, \tag{7}$$

where $r_i^{ab}(i = 1, 2)$ is the reflection coefficient, in which a and b are the polarization of incident and reflected waves, respectively.

Thus, we can finally deduce the radiative heat transfer straightforwardly from the electric Green's dyadic. The calculation procedure has been established for isotropic and anisotropic media.[2,18] We will not repeat the derivations here. The final form of spectral radiative heat transfer is

$$\begin{aligned}S_\omega = {}& [\Theta(\omega, T_2) - \Theta(\omega, T_1)]\\ &\times \left\{\int_{\mathrm{k}_{||}<k_0}\frac{\mathrm{k}_{||}d\mathrm{k}_{||}}{(2\pi)^2}\mathrm{Tr}\left[(\mathbf{I} - \mathbf{R}_2^*\mathbf{R}_2)\mathbf{D}_{12}(\mathbf{I} - \mathbf{R}_1\mathbf{R}_1^*)\mathbf{D}_{12}^*\right]\right.\\ &\left. + \int_{\mathrm{k}_{||}>k_0}\frac{\mathrm{k}_{||}d\mathrm{k}_{||}}{(2\pi)^2}\mathrm{Tr}\left[(\mathbf{R}_2^* - \mathbf{R}_2)\mathbf{D}_{12}(\mathbf{R}_1 - \mathbf{R}_1^*)\mathbf{D}_{12}^*\mathrm{e}^{-2|\gamma|d}\right]\right\},\end{aligned} \tag{8}$$

where $\Theta(\omega, T_i) = \hbar\omega/(\exp(\hbar\omega/k_BT_i) - 1)$, Tr is the trace operator, and the symbol * denotes the hermitian conjugation. For chiral media, the elements in $\mathbf{R}_i$ are[34]

$$r_i^{ss} = \frac{-\Gamma_-(\xi_+ + \xi_-) - (\xi_+\xi_- - 1)}{\Gamma_+(\xi_+ + \xi_-) + (\xi_+\xi_- + 1)}, \tag{9a}$$

$$r_i^{pp} = \frac{\Gamma_-(\xi_+ + \xi_-) - (\xi_+\xi_- - 1)}{\Gamma_+(\xi_+ + \xi_-) + (\xi_+\xi_- + 1)}, \tag{9b}$$

$$r_i^{sp} = -r_i^{ps} = \frac{i(\xi_+ - \xi_-)}{\Gamma_+(\xi_+ + \xi_-) + (\xi_+\xi_- + 1)}, \tag{9c}$$

where $\Gamma_\pm = (\eta_0^2 \pm \eta_i^2)/2\eta_0\eta_i$, $\xi_\pm = \gamma_\pm/n_\pm\gamma$, $\eta_0 = \sqrt{\mu_0/\varepsilon_0}$, $\eta_i = \sqrt{\mu_0\mu_i/\varepsilon_0\varepsilon_i}$, $\gamma_\pm = \sqrt{n_\pm^2k_0^2 - \mathrm{k}_{||}^2}$, and $n_\pm = \sqrt{\varepsilon_i\mu_i} \pm \kappa_i$. Note that when $\kappa = 0$, Eqs. (9) will reduce to the usual reflection coefficients

$$r_i^{ss} = \frac{\mu_i\sqrt{k_0^2 - \mathrm{k}_{||}^2} - \sqrt{\varepsilon_i\mu_ik_0^2 - \mathrm{k}_{||}^2}}{\mu_i\sqrt{k_0^2 - \mathrm{k}_{||}^2} + \sqrt{\varepsilon_i\mu_ik_0^2 - \mathrm{k}_{||}^2}}, \tag{10a}$$

$$r_i^{pp} = \frac{\varepsilon_i\sqrt{k_0^2 - \mathrm{k}_{||}^2} - \sqrt{\varepsilon_i\mu_ik_0^2 - \mathrm{k}_{||}^2}}{\varepsilon_i\sqrt{k_0^2 - \mathrm{k}_{||}^2} + \sqrt{\varepsilon_i\mu_ik_0^2 - \mathrm{k}_{||}^2}}, \tag{10b}$$

$$r_i^{sp} = -r_i^{ps} = 0, \tag{10c}$$

where we find that the non-diagonal elements are zero. This is because at the interface of the non-chiral media and vacuum, the polarization of reflected waves is the same with the incident waves. However, when the waves (s- or p-polarization) are probed into the surface of the chiral material, the reflected waves will be a mixture of both polarizations. For non-chiral materials, Eq. (8) will reduce to the well known formula

$$\begin{aligned}S_\omega^0 = {}& [\Theta(\omega, T_2) - \Theta(\omega, T_1)]\\ &\times \sum_{j=s,p}\left\{\int_{\mathrm{k}_{||}<k_0}\frac{\mathrm{k}_{||}d\mathrm{k}_{||}}{4\pi^2}\frac{(1 - |r_1^j|^2)(1 - |r_2^j|^2)}{|1 - r_1^jr_2^j\mathrm{e}^{-2|\gamma|d}|^2}\right.\\ &\left. + \int_{\mathrm{k}_{||}>k_0}\frac{\mathrm{k}_{||}d\mathrm{k}_{||}}{\pi^2}\frac{\mathrm{Im}(r_1^j)\mathrm{Im}(r_2^j)\mathrm{e}^{-2|\gamma|d}}{|1 - r_1^jr_2^j\mathrm{e}^{-2|\gamma|d}|^2}\right\}.\end{aligned} \tag{11}$$

To gain a deeper insight into the effect of chirality on near-filed radiative heat transfer, we compare our formula with Eq. (11). For clarity of discussion, we expand the trace operation in the integrand of Eq. (8) for $\mathrm{k}_{||} > k_0$

$$T(\omega,\mathrm{k}_{||},d)=\mathrm{Tr}[(\mathbf{R}_2^*-\mathbf{R}_2)\mathbf{D}_{12}(\mathbf{R}_1-\mathbf{R}_1^*)\mathbf{D}_{12}^*\mathrm{e}^{-2|\gamma|d}]=2\begin{bmatrix}\mathrm{Im}(r_1^{ss})\mathrm{Im}(r_2^{ss})|D_{pp}|^2+\mathrm{Im}(r_1^{pp})\mathrm{Im}(r_2^{ss})|D_{ps}|^2\\+\mathrm{Re}(r_1^{sp})\mathrm{Re}(r_2^{sp})\mathrm{Re}(D_{pp}D_{ss}^*+D_{ps}D_{sp}^*)\\+4\,\mathrm{Im}(r_2^{ss})\mathrm{Re}(r_1^{sp})\mathrm{Im}(D_{pp}D_{ps}^*)+(1\leftrightarrow 2,s\leftrightarrow p)\end{bmatrix}\frac{\mathrm{e}^{-2|\gamma|d}}{|\Delta|^2},\quad(12)$$

with

$$D_{pp}=1-(r_1^{pp}r_2^{pp}-r_1^{sp}r_2^{sp})\mathrm{e}^{-2|\gamma|d},$$
$$D_{ss}=1-(r_1^{ss}r_2^{ss}-r_1^{sp}r_2^{sp})\mathrm{e}^{-2|\gamma|d},$$
$$D_{ps}=(r_1^{ss}r_2^{sp}+r_2^{pp}r_1^{sp})\mathrm{e}^{-2|\gamma|d},\quad D_{sp}=(r_1^{pp}r_2^{sp}+r_2^{ss}r_1^{sp})\mathrm{e}^{-2|\gamma|d},$$
$$\Delta=1-(r_1^{ss}r_2^{ss}+r_1^{pp}r_2^{pp}-2r_1^{sp}r_2^{sp})\mathrm{e}^{-2|\gamma|d}+(r_1^{sp}r_1^{sp}+r_1^{ss}r_1^{pp})(r_2^{sp}r_2^{sp}+r_2^{ss}r_2^{pp})\mathrm{e}^{-4|\gamma|d}.$$

$T(\omega,\mathrm{k}_{||},d)$ is the transmission factor of the two-interface system, and $(a\leftrightarrow b)$ denotes the terms obtained by interchanging the index a and b.

It is clear from the comparison of Eq. (12) and Eq. (11) that the additional terms are attributed to the off-diagonal matrix elements r_i^{sp} and r_i^{ps}. Also due to r_i^{sp} and r_i^{ps}, the terms in Eq. (12) about s- and p-polarization are mixed and cannot be separated in the way shown in Eq. (11). Moreover, a direct transformation of Eq. (9c) shows that the modulus of r_i^{sp} and r_i^{ps} are proportional to κ. As known that for non-chiral media, surface modes mediated heat transfer is attributed to either s- or p-polarization; here, we find that in chiral material the effect of surface modes is chirality-dependent and cross-coupled via the contributions of both polarizations.

Furthermore, regarding the near-field contribution only, it is shown that the photon tunneling of evanescent modes is modulated when chirality is taken into account. This is because that in Eq. (11), two physically meaningful components combine to form the transmission factor of evanescent waves. The numerator part corresponds to the overlap of local density of state (LDOS) defined as $\mathrm{Im}(r_1^j)\mathrm{e}^{-2|\gamma|d}$. The Fabry-Pérot-type denominator, $1-r_1^jr_2^j\mathrm{e}^{-2|\gamma|d}$, corresponds to the contribution of MRs between two semi-infinite surfaces. As shown in Eq. (12), both the components of the LDOS and MRs are modified and the quantity of modification can be either positive or negative for both components. Thus, one may wonder whether controlling chirality can bring new features into the enhanced radiative heat transfer.

III. RESULTS AND ANALYSIS

Now, we present some numerical results obtained with two CMMs. The optical properties can be described using an Ω-particle resonator model[36]

$$\varepsilon(\omega)=1-\frac{X_\varepsilon\omega_0^2}{\omega^2-\omega_0^2+i\Upsilon\omega},\quad(13a)$$

$$\mu(\omega)=1+X_\mu-\frac{X_\mu\omega^2}{\omega^2-\omega_0^2+i\Upsilon\omega},\quad(13b)$$

$$\kappa(\omega)=\frac{X_\kappa\omega\omega_0}{\omega^2-\omega_0^2+i\Upsilon\omega},\quad(13c)$$

where X_ε and X_μ are coefficients that represent the strength of permittivity and permeability, respectively, X_κ is the chirality coefficient characterizing the strength of magnetoelectric coupling effect, ω_0 is the resonant frequency, and Υ is the scattering rate.

Here, some remarks on Eqs. (13) are necessary. As artificial materials, the optical properties of metamaterials can be controlled by tuning X_ε, X_μ, X_κ, ω_0, and Υ, since these coefficients are intimately related to the geometrical size and configuration of the unit-cell. On the other hand, there exists fundamental limit for the value of chirality. Based on the second law of thermodynamics, heat liberated per unit volume in a passive material must be positive. For harmonic electromagnetic fields, the average value of heat liberated is $q=\mathrm{Im}\{\omega(\mathrm{E}^\dagger\cdot\mathrm{D}+\mathrm{H}^\dagger\cdot\mathrm{B})/2\}$; substituting the constitutive relations into this expression and setting $q>0$, we obtain that the lossy component of the constitute parameters must obey[37]

$$\mathrm{Im}(\varepsilon)\mathrm{Im}(\mu)\geq\mathrm{Im}^2(\kappa).\quad(14)$$

Substituting Eqs. (13) into (14), we find the up-limit of X_κ

$$X_\kappa{}^2\leq X_\varepsilon X_\mu.\quad(15)$$

We first study the dependence of spectral radiative heat transfer on the strength of magnetoelectric coupling X_κ. In Fig. 1 we show the reduced spectral heat transfer between two identical CMMs, S_ω/S_{BB}, where S_{BB} is the heat transfer between two blackbodies. This quantity is dimensionless and can be viewed as the heat transfer enhancement over the blackbody radiation limit. In our calculation, we introduce a dimensionless distance $d_r=d/\lambda_0$ with $\lambda_0=2\pi c/\omega_0$ and plot the figures as the function of ω/ω_0. In such case, the reduced spectral heat transfer would be independent of the specific value of ω_0. Without loss of generality, the parameters are taken as $X_\varepsilon=2$, $X_\mu=0.5$, and $d_r=0.001$ in Fig. 1. The influence of the dissipation effect on the near-field heat flux is included by considering different scattering rates.

Remarkably, we find in Fig. 1(a) that the near-field heat flux peaks are shifted in the presence of magnetoelectric coupling, and stronger coupling leads to larger peak-frequency distance. This spectral effect can be explained from the following analysis. Recall that the heat flux peaks in non-chiral case are at the resonant frequencies of SPs, which satisfy $\varepsilon(\omega)=-1$ and $\mu(\omega)=-1$ for p- and s-polarization waves, respectively.[26] In chiral case, however, magnetoelectric coupling effect mixes the contributions of both polarizations. The dispersion relation of surface modes corresponds to the pole of the reflection coefficients in Eqs. (9)

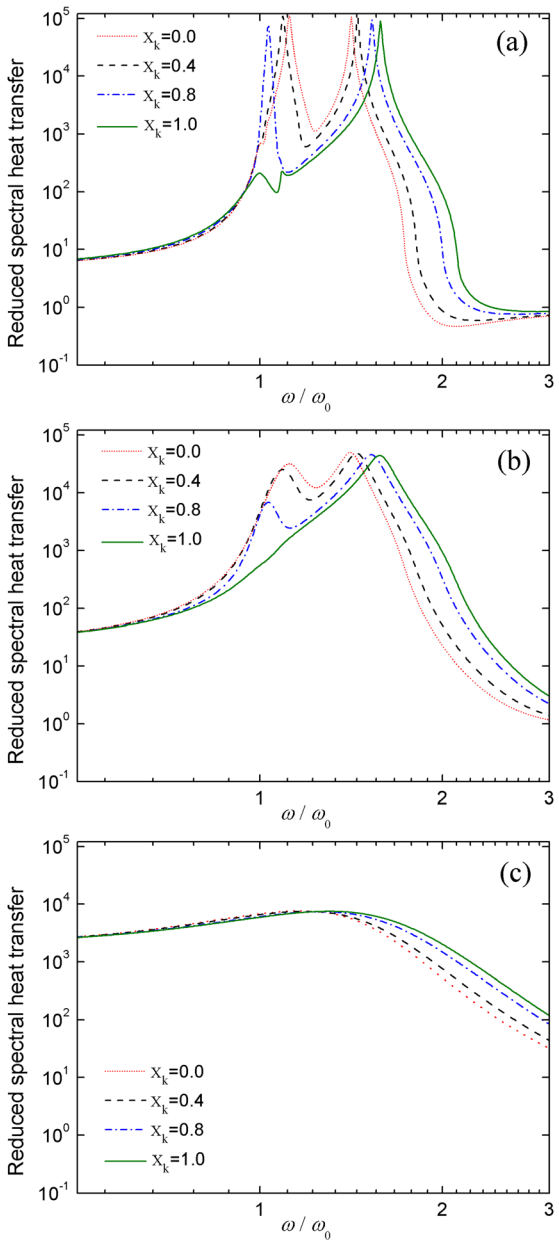

FIG. 1. Reduced spectral radiative heat transfer between two identical chiral metamaterials at different strength of magnetoelectric coupling X_κ and $d_r = 0.001$. The transfer is calculated for scattering rate (a) $\Upsilon = 0.01\omega_0$, (b) $\Upsilon = 0.1\omega_0$, and (c) $\Upsilon = \omega_0$.

$$\Gamma_+(\xi_+ + \xi_-) + (\xi_+\xi_- + 1) = 0. \tag{16}$$

The heat flux peaks correspond to the resonances of surface modes, which obey

$$[\varepsilon(\omega) + 1][\mu(\omega) + 1] = \kappa^2(\omega). \tag{17}$$

The peak frequencies can be solved by substituting Eqs. (13) into (17)

$$\omega_{c\pm}^2 = \omega_\pm^2 \pm \frac{1}{8}\omega_0^2\Big[\pm X_\kappa^2 - 2|X_\varepsilon - X_\mu| + \sqrt{X_\kappa^4 + 4X_\kappa^2(4 + X_\varepsilon + X_\mu) + 4(X_\varepsilon - X_\mu)^2}\Big], \tag{18}$$

where $\omega_\pm = \omega_0\sqrt{1 + (X_\varepsilon + X_\mu \pm |X_\varepsilon - X_\mu|)/4}$ corresponds to the peak frequencies in non-chiral case. The peak-frequency distance $\Delta\omega_c^2 = \omega_{c+}^2 - \omega_{c-}^2$ is

$$\Delta\omega_c^2 = \Delta\omega^2 + \frac{1}{4}\omega_0^2\Big[-2|X_\varepsilon - X_\mu| + \sqrt{X_\kappa^4 + 4X_\kappa^2(4 + X_\varepsilon + X_\mu) + 4(X_\varepsilon - X_\mu)^2}\Big], \tag{19}$$

where $\Delta\omega^2 = \omega_+^2 - \omega_-^2$. From Eqs. (18) and (19), we can see that the SPs are dependent of the effect of magnetoelectric coupling, and the phenomena of shifted peak frequencies and amplified peak-frequency distance in Fig. 1(a) can be easily deduced. Since X_κ is limited by the thermodynamic condition, there exist up and low limit for the peak frequency. By substituting $X_\varepsilon X_\mu = X_\kappa^2$ into Eq. (18), we get $\omega_c^{up} = \omega_0\sqrt{(X_\varepsilon + 2)(X_\mu + 2)}/2$ and $\omega_c^{low} = \omega_0$.

Figure 1(a) also shows the dependence of the peak strength and the half-peak width on the magnetoelectric coupling strength X_κ. The two quantities represent the influence of dissipation on the surface modes mediated heat transfer. From Eqs. (13), dissipation (which can be seen from the imaginary part of constitute parameters) originates from non-zero scattering rate and can be modulated by adjusting either the scattering rate or the other coefficients in Eqs. (13). For the case of dielectrics, the influence of scattering rate on heat transfer has been discussed in Ref. 38, in which other coefficients are kept constant. It is shown that smaller scattering rate leads to sharper peak and narrower width. In comparison, here we find that when scattering rate is kept constant, the peak strength and the spectral width exhibit different behaviors. First, both the low and high frequency peaks decrease in strength as X_κ increases. Moreover, the low frequency peak behaves more sensitive to the change of X_κ than the high frequency peak. Especially, the magnitude of the low frequency peak is decreased by more than 2 orders when X_κ approaches 1.0. Explanation of this behavior is direct. From Eq. (18), when $X_\kappa \to 1.0$, the low frequency surface modes are exhibited at $\omega \to \omega_0$. Note that near the resonant frequency ω_0, large dissipation is induced due to very larger value of the imaginary part of constitutive parameters. Hence, the contribution of the surface modes to heat transfer would be significantly weakened due to the strong absorption of surface waves. In such case, the heat flux peak is largely attributed to the large refraction index ($n = \sqrt{\varepsilon\mu} \pm \kappa$) of material. Otherwise, inspection of the half-peak width in Fig. 1(a) shows that the low frequency peak becomes narrow as X_κ increases (except at $X_\kappa = 1.0$, the peak is weak and broad). In contrast, the width of the high frequency peak is independent of X_κ. This is notably different from what is shown in the case when the spectral width varies with the scattering rate. The mechanism involved in this behavior still remains an open question. However, we can speculate by comparing the difference of the two peaks that the interaction of the low frequency surface modes and the large dissipation effect near the resonant frequency plays an important role in this behavior.

Figures 1(b) and 1(c) show the influence of the scattering rate on the spectral heat transfer. For low scattering rate ($\Upsilon = 0.01\omega_0$), the peak strength of the heat flux is found to be ~5 orders of magnitude larger than the blackbody radiation limit. In contrast, it is decreased by ~1 order of magnitude for $\Upsilon = \omega_0$. Meanwhile, the half-peak width of the spectral curve becomes broader as the scattering rate increases. Since the heat flux peaks are attributed to the resonances of surface modes, it can seen that in the presence of large scattering rate, the heat transfer channel of surface modes is greatly dissipated. In particular, at $\Upsilon = \omega_0$, only the high frequency peak is exhibited since the resonance of the low frequency surface modes has been fully suppressed (note that here we identify the high frequency peak by the direction of the peak shift). However, it should be pointed out that though the sharp heat flux peaks decrease as the scattering rate increases, it does not equivalently mean that a lower scattering rate is beneficial for increasing the total heat transfer. For low scattering rate [see Fig. 1(a)], the heat energy is transferred mainly through frequencies around the resonances of surface modes, and the contribution from the regions of $\omega/\omega_0 > 3$ and $\omega/\omega_0 < 0.5$ has been negligible. However, when the scattering rate increases, a broad-band enhancement of spectral heat transfer occurs. Indeed, in such case, the broad-band enhancement leads to larger total heat transfer than the narrow-band enhancement at low scattering rate [shown below].

Figure 2 shows the evolving of reduced spectral heat transfer with respect to X_k and separation distances. Two principle peaks induced by SPs can be identified, which occur at fixed frequencies when the separation distance varies. Unlike the SP-induced peaks, we also observe a novel type of peaks at intermediate and strong chirality. For this type of non-SP-induced peaks, we find a peak-displacement phenomenon, depending on the separation distance, as shown more clearly in Fig. 2(d).

For the origin of the non-SP-induced peak, we consider the resonant photon tunneling of evanescent waves. Note that in the photon tunneling process, only tunneling modes with small $k_{||}$ can undergo several times of MRs due to that the propagation distance is $l \propto k_{||}^{-1}$. The resonant behavior of MRs is shown in the denominator of Eq. (12), i.e., $\Delta = 1 - (r_{ss}^2 + r_{pp}^2 - 2r_{sp}^2)e^{-2|\gamma|d} + (r_{sp}^2 + r_{ss}r_{pp})^2 e^{-4|\gamma|d}$. Figure 3 displays the logarithmic contour plots of $1/|\Delta|^2$, for non-chiral media and CMMs, respectively. The dark line that corresponds to the minima of $1/|\Delta|^2$ results from very large reflection coefficients at the resonant frequency of SP. The light branches that correspond to the maxima of $1/|\Delta|^2$ is due to the resonance of MRs at $\Delta \to 0$. It is seen that the contribution of evanescent waves at small $k_{||}$ diverges for materials with different properties. Compared with Fig. 3(a), we observe that the lower light branch in Fig. 3(b) becomes flat for a limited interval of $k_{||}$ (the dashed line). This thus leads to an enhanced contribution to heat transfer at the corresponding frequency. Since large $k_{||}$ also has a strong impact upon radiative heat transfer, therefore, the radiative heat transfer is governed by the competition between the enhanced contribution at small $k_{||}$ and the contribution of large $k_{||}$. Indeed, the observable effect of small $k_{||}$ modes, i.e., the non-SP-induced heat flux peaks, can only appear in the presence of strong magnetoelectric coupling.

It is clear from the above results that the contribution of the small $k_{||}$ modes and large $k_{||}$ is due to different physical mechanisms. For large $k_{||}$, $\gamma = \gamma_{\pm} \approx i k_{||}$. Hence, the reflection coefficients can be asymptotically reduced to $r_{ss} \approx [(\varepsilon+1)(\mu-1) - \kappa^2]/\Pi$, $r_{pp} \approx [(\varepsilon-1)(\mu+1) - \kappa^2]/\Pi$,

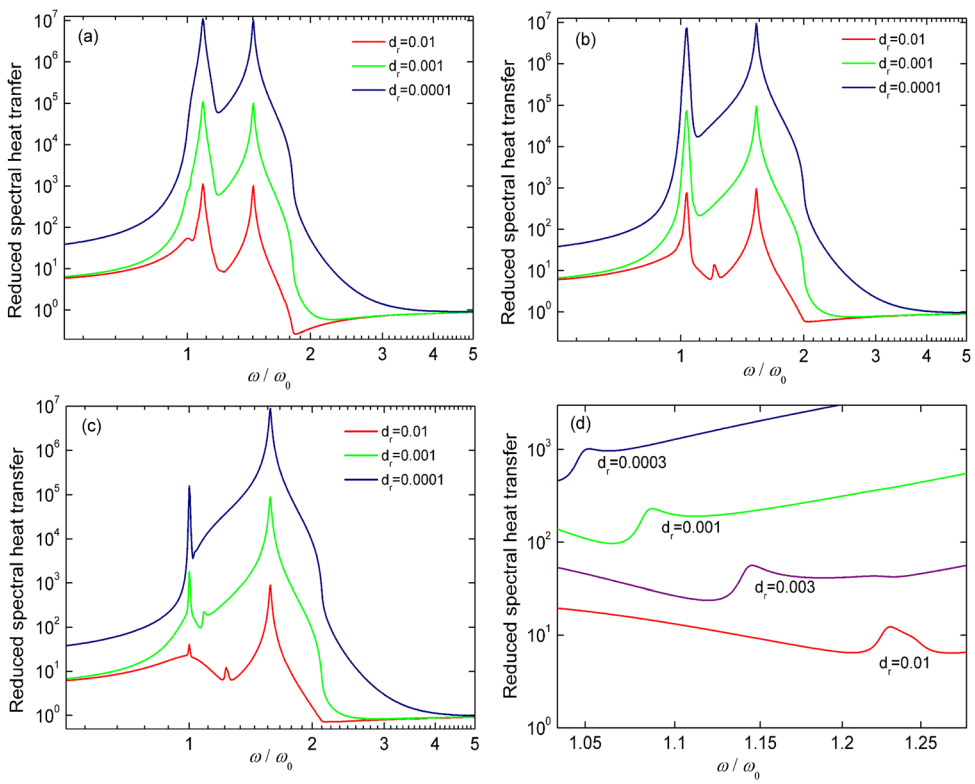

FIG. 2. Spectral evolving of reduced radiative heat transfer at different separation distances and $\Upsilon = 0.01\omega_0$ for (a) $X_\kappa = 0.4$, (b) $X_\kappa = 0.8$, and (c) $X_\kappa = 0.95$. (d) Distance-dependent peak displacement behavior of non-SP-induced peaks at $X_\kappa = 0.95$.

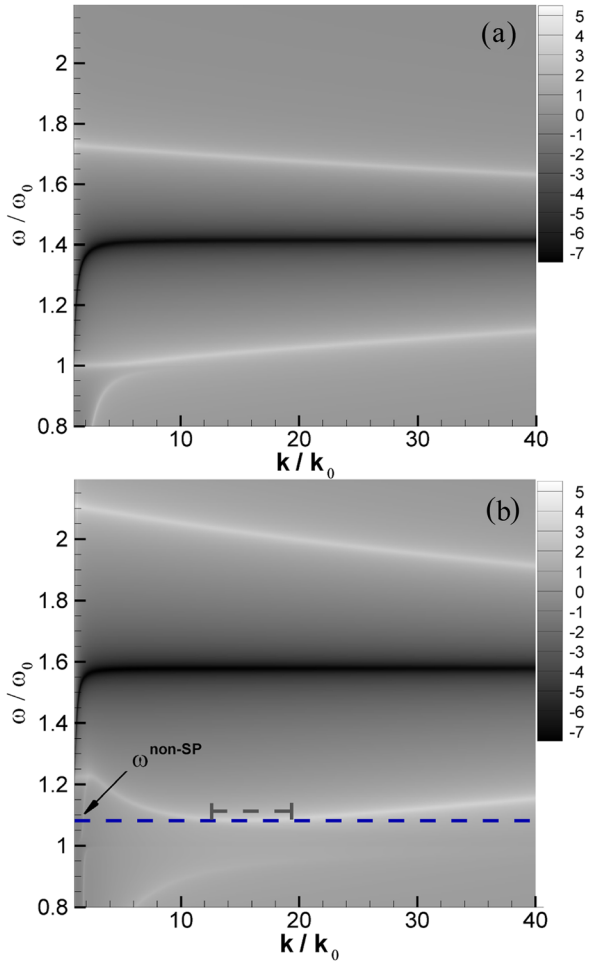

FIG. 3. Logarithmic contour plot of $1/|\Delta|^2$, $\Delta = 1 - (r_{ss}^2 + r_{pp}^2 - 2r_{sp}^2)\,e^{-2|\gamma|d} + (r_{sp}^2 + r_1^{ss} r_1^{pp})^2 e^{-4|\gamma|d}$ for (a) non-chiral materials, and (b) CMMs at $X_\kappa = 0.95$, $d_r = 0.001$, and $\Upsilon = 0.01\omega_0$. The gray dashed lines represent the zone where small $k_{||}$ modes at a certain frequency give enhanced contribution to heat transfer. The blue dashed line corresponds to the non-SP-induced peak frequency.

and $r_{sp} \approx -2\kappa i/\Pi$, where $\Pi = (\varepsilon + 1)(\mu + 1) - \kappa^2$. Since $\Pi = 0$ corresponds to the resonant frequencies of the SPs, the radiative heat transfer is greatly enhanced due to high LDOS in the presence of surface modes. Nevertheless, small $k_{||}$ modes contribute only in the presence of strong magnetoelectric coupling. In this case, the tunneling photons are effectively multiple-reflected within the vacuum gap, exhibiting a resonant tunneling event at a certain frequency.

In Fig. 4, we plot the non-SP-induced peak frequency ω^{non-SP} and the peak strength as the function of separation distance. When separation distance increases, the peak displaces to high frequency. For this behavior, it might be due to the sensitivity of the resonant tunneling condition to distance at small $k_{||}$, which is shown in the $e^{-2|\gamma|d}$ term of the denominator of transmission factor. Moreover, we find that the non-SP-induced peak strength varies as d^a with $-2 < a < -1$ in the near-field regime ($d_r \lesssim 0.008$). To enhance the contribution of this channel, as seen in Figs. 2 and 4, we can decrease the separation distance or increase the magnetoelectric coupling. Also, it shows that the increasing rate of heat transfer through this channel is lower than

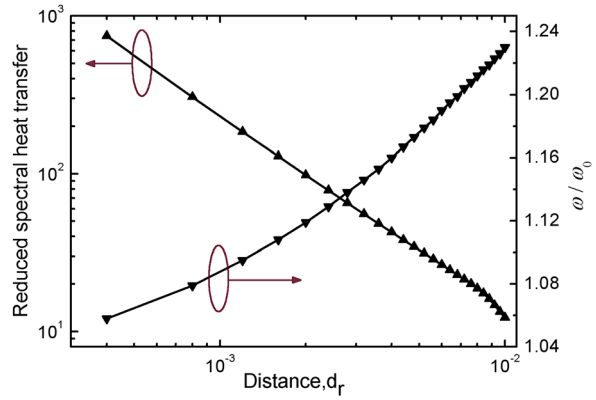

FIG. 4. Frequency of non-SP-induced peak and the reduced spectral radiative heat transfer at ω^{non-SP} vs distance at $X_\kappa = 0.95$ and $\Upsilon = 0.01\omega_0$.

that through the SP-induced channels (which vary as d^{-2}), so it is understandable that within ultra-short distance (at $d_r \lesssim 0.001$) the non-SP-induced peaks vanish and the SPs dominate the radiative heat transfer.

Finally, we analyze the behavior of total radiative heat transfer coefficients with respect to the separation distance. The heat transfer coefficient is defined as

$$h = \lim_{T_1 \to T_2} \frac{\int_0^\infty S_\omega(T_1, T_2, d)\, d\omega}{T_2 - T_1}, \tag{20}$$

where S_ω is spectral heat transfer defined in Eq. (8). To quantify the heat transfer enhancement, the results are normalized to the heat transfer coefficient of blackbody radiation $h_0 = 4\sigma T^3$. In our calculation, we set $\omega_0 = 3 \times 10^{14}$ rad/s and $T = 300$ K. Figure 5(a) shows that the heat transfer coefficient decreases monotonically as X_κ increases. For small separation ($d_r \lesssim 0.003$), the heat transfer coefficients of non-chiral metamaterial and CMM with weak chirality are ~1 order of magnitude larger than that of CMM with $X_\kappa = 1.0$. This difference vanishes at large separation, indicating that chirality effect is only relevant in ultra-short near-field regime. On the other hand, the influence of scattering rate on heat transfer coefficients is illustrated in Figs. 5(b) and 5(c). It is seen that the heat transfer difference between non-chiral metamaterial and CMM is greatly narrowed as the scattering rate increases. Moreover, inspection of the curves shows that given the chirality, near-field heat transfer at large scattering rate is much greater than that at small scattering rate. For example, at $d_r = 0.001$ and $X_\kappa = 1.0$, the heat transfer coefficient for $\Upsilon = \omega_0(\sim 3500)$ is 5 and 17 times larger than the coefficients for $\Upsilon = 0.1\omega_0(\sim 700)$ and $\Upsilon = 0.01\omega_0(\sim 200)$. As we know, very low scattering rate is necessary for frequency-selective enhancement of heat transfer, i.e., several orders of magnitude enhancement occurring at resonant frequency of surface modes. However, here it shows that there exists tradeoff between the frequency selectivity and the overall enhancement of heat transfer.

IV. DISCUSSION

In this section, we make some discussions on the near-field thermal applications of CMMs. According to the numerical

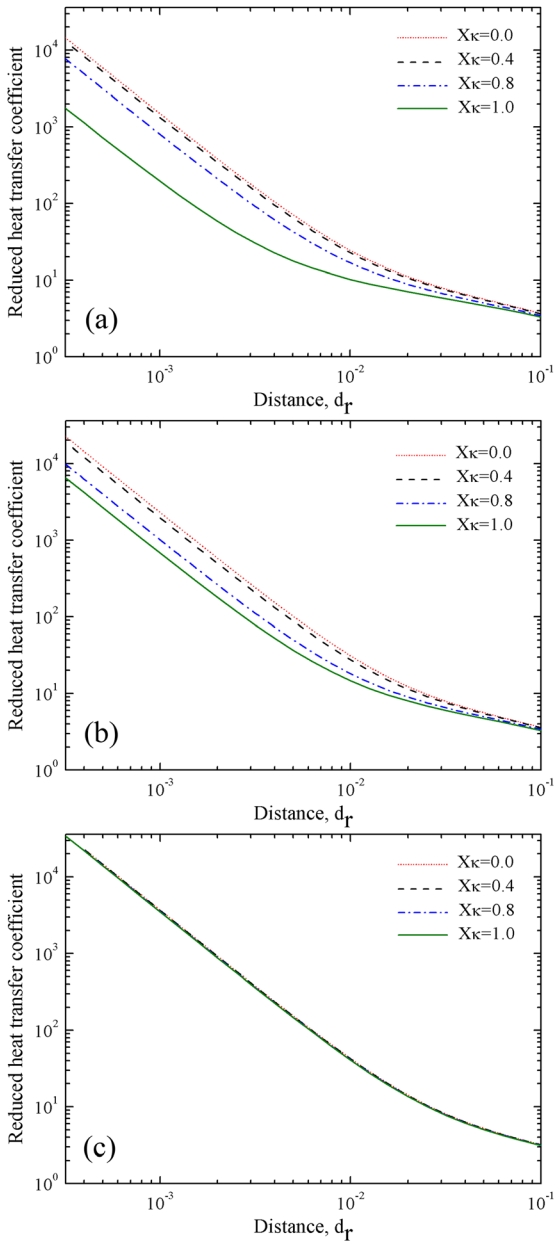

FIG. 5. Reduced total heat transfer coefficient vs distance for different strength of magnetoelectric coupling at $T_{1,2} = 300$K. The transfer is calculated for scattering rate taking as (a) $\Upsilon = 0.01\omega_0$, (b) $\Upsilon = 0.1\omega_0$, and (c) $\Upsilon = \omega_0$.

results, the heat transfer through the channels of the surface modes is greatly enhanced and strongly chirality-dependent. For practical purpose, this effect can be exploited to make CMM as a thermal emitter in designing thermophotovoltaic (TPV) system, as an addition to the reported TPV emitter using near-field surface mode of dielectrics.[39] The essential mechanism is to design the metamaterial in which the resonance of surface modes is exhibited in the sensitive frequency region of the TPV cell, i.e., the band gap energy of the semiconductor. This will make a better energy match between the thermal emitter and the photovoltaic cell and thus leads to high performance of energy conversion. However, in order to apply this structure, some comments on the integrity of metamaterials at high temperatures (TPV emitter often works between 1000 K and 2000 K) are necessary. To design artificial materials with stable optical and mechanical properties at high temperatures is a challenging problem. Metamaterial structure often consists of an array of metallic resonator elements fabricated on a dielectric substrate. When such structure operates at high temperatures, unfavorable physical changes (e.g., melting, evaporation, or thermally induced mechanical deformation) or chemical reactions between different materials may be inevitable. Moreover, the diffusion of unstable surface atoms can change the roughness and optical property of surface and thus influences the thermal radiation property of the structure. To overcome the above challenges, selecting proper constituent materials to construct metamaterial is a key step. Recently reported metamaterial designs[40,41] have employed materials with high thermal stability, such as silicon carbide, tungsten, and aluminum nitride. These proposals have shed some new lights on metamaterials that can be effectively used as a TPV emitter.

Besides the application in near-field energy conversion, another application is about the experimental realization of near-field heat transfer. As well known, the experiments of near-field heat transfer have remained difficult since the heat transfer is dominated by the localized evanescent modes, which are significant within submicron scale. Because the heat flux is strongly dependent on the separation distance, in such small distances, the precise calibration of distance is crucial. Indeed, all currently reported experiments apply feedback control scheme to keep a constant separation distance. Here, we provide an alternative distance-calibration approach which can be used as an auxiliary method in near-field heat transfer experiments. This is based on the findings in Fig. 2(d), in which we observe a displacement phenomenon of heat flux peaks when the separation distance varies. The relation between the separation distance and the non-SP-induced peak frequency is quantified in Fig. 4. In other words, the distance can thus be precisely determined by measuring the corresponding peak frequency. It has been shown in recent measurement[42] of near-field spectral distribution that thermal signal can be captured with very high sensitivity. Therefore, though the non-SP-induced peak is very weak compared with the SP-induced peaks, its magnitude has been high enough to be observed.

Finally, we discuss the influence of the metamaterial fabrication on near-field thermal applications. Fabricating metamaterials with electromagnetic response at infrared and visible frequency regions is a challenging problem. Such metamaterials consist of unit-cells that possess complex structures within submicron- and nano-scale. Recent studies have shown that by advanced top-down and down-top nanotechnology, chiral metamaterial can be realized at frequency up to THz[43] and infrared region.[44] On the other hand, the fabrication of metamaterials is also plagued by dissipative loss, which often increases with the response frequency. The loss in metamaterial originates from both the constituent materials and the fabrication process. The dissipation effect has significant influence on near-field heat transfer. We have shown above that large scattering rate (large dissipation) counteracts the contribution of chirality effect. Thus, for applications which require chirality-dependent behaviors, metamaterial structures with large dissipation will be

ineffective. However, compared with metamaterials with low dissipation, large dissipation can lead to much larger enhancement of total heat transfer. This implies that though large dissipation structure is often ruled out in many optical applications, it could be optimal in near-field thermal applications that prefer total heat transfer as large as possible.

V. CONCLUSION

In conclusion, we have shown that the surface polariton mediated near-field heat transfer is modulated when magnetoelectric coupling effect is involved in this transfer. We demonstrate that in the presence of strong coupling effect, a novel heat transfer channel is activated by the resonant tunneling modes with small wavenumbers. We also find that the scattering rate, which characterizes the dissipative power in material, significantly influences the effect of magnetoelectric coupling on heat transfer. These emerging behaviors can be exploited in applications of near-field TPV energy conversion and the experimental realizations of near-field radiative heat transfer.

ACKNOWLEDGMENTS

Y.H. gratefully acknowledges support from the Fundamental Research Funds for the Central Universities (No. YWF-11-03-Q-028).

[1]K. Joulain, J.-P. Mulet, F. Marquier, R. Carminati, and J.-J. Greffet, Surf. Sci. Rep. **57**, 59 (2005).
[2]A. I. Volokitin and B. N. J. Persson, Rev. Mod. Phys. **79**, 1291 (2007).
[3]S. Basu, Z. M. Zhang, and C. J. Fu, Int. J. Energy Res. **33**, 1203 (2009).
[4]S. M. Rytov, Y. A. Kravtsov, and V. I. Tatarskii, *Principles of Statistical Radiophysics* (Springer-Verlag, Berlin, 1989), Vol. 3.
[5]G. Domingues, S. Volz, K. Joulain, and J.-J. Greffet, Phys. Rev. Lett. **94**, 085901 (2005).
[6]A. I. Volokitin and B. N. J. Persson, Phys. Rev. B **63**, 205404 (2001).
[7]A. Narayanaswamy and G. Chen, Phys. Rev. B **77**, 075125 (2008).
[8]A. W. Rodriguez, O. Ilic, P. Bermel, I. Celanovic, J. D. Joannopoulos, M. Soljacic, and S. G. Johnson, Phys. Rev. Lett. **107**, 114302 (2011).
[9]P. Ben-Abdallah, S.-A. Biehs, and K. Joulain, Phys. Rev. Lett. **107**, 114301 (2011).
[10]C. Otey and S. Fan, Phys. Rev. B **84**, 245431 (2011).
[11]P. Ben-Abdallah, K. Joulain, J. Drevillon, and G. Domingues, J. Appl. Phys. **106**, 044306 (2009).
[12]M. Francoeur, M. P. Mengüc, and R. Vaillon, Phys. Rev. B **84**, 075436 (2011).
[13]M. Krüger, Th. Emig, and M. Kardar, Phys. Rev. Lett. **106**, 210404 (2011).
[14]I. Volokitin and B. N. J. Persson, Phys. Rev. B **83**, 241407(R) (2011).
[15]J. van Zwol, K. Joulain, P. Ben Abdallah, J. J. Greffet, and J. Chevrier, Phys. Rev. B **83**, 201404(R) (2011).
[16]C. J. Fu and Z. M. Zhang, Int. J. Heat Mass Transfer **49**, 1703 (2006).
[17]Z. Zheng and Y. Xuan, Int. J. Heat Mass Transfer **54**, 1101 (2011).
[18]S.-A. Biehs, P. Ben-Abdallah, F. S. S. Rosa, K. Joulain, and J.-J. Greffet, Opt. Express **19**, A1088 (2011).
[19]A. Narayanaswamy, S. Shen, and G. Chen, Phys. Rev. B **78**, 115303 (2008).
[20]E. Rousseau, A. Siria, G. Jourdan, S. Volz, F. Comin, J. Chevrier, and J.-J. Greffet, Nat. Photonics **3**, 514 (2009).
[21]R. S. Ottens, V. Quetschke, S. Wise, A. A. Alemi, R. Lundock, G. Mueller, D. H. Reitze, D. B. Tanner, and B. F. Whiting, Phys. Rev. Lett. **107**, 014301 (2011).
[22]Y. De Wilde, F. Formanek, R. Carminati, B. Gralak, P.-A. Lemoine, K. Joulain, J.-P. Mulet, Y. Chen, and J.-J. Greffet, Nature (London) **444**, 740 (2006).
[23]C. R. Otey, W. T. Lau, and S. Fan, Phys. Rev. Lett. **104**, 154301 (2010).
[24]B. J. Lee, Y.-B. Chen, and Z. M. Zhang, J. Quantum Spectrosc. Radiat. Transfer **109**, 608 (2008).
[25]J. L. Pan, H. K. Choy, and C. G. Fonstad, IEEE Trans. Electron Devices **47**, 241 (2000).
[26]K. Joulain, J. Drevillon, and P. Ben-Abdallah, Phys. Rev. B **81**, 165119 (2010).
[27]M. Francoeur, S. Basu, and S. J. Petersen, Opt. Express **19**, 18774 (2011).
[28]S. Basu and M. Francoeur, Appl. Phys. Lett. **99**, 143107 (2011).
[29]J. Pendry, A. J. Holden, D. J. Robbins, and W. J. Stewart, IEEE Trans. Microwave Theory Tech. **47**, 2075 (1999).
[30]J. B. Pendry, Science **306**, 1353 (2004).
[31]S. Tretyakov, I. Nefedov, A. Sihvola, S. Maslovski, and C. Simovski, J. Electromagn. Waves Appl. **17**, 695 (2003).
[32]C. Monzon and D. W. Forester, Phys. Rev. Lett. **95**, 123904 (2005).
[33]G. Chen, *Nanoscale Energy Transport and Conversion: A Parallel Treatment of Electrons, Molecules, Phonons, and Photons* (Oxford University Press, New York, 2005).
[34]A. Lakhtakia, *Beltrami Fields in Chiral Media* (World Scientific, Singapore, 1994).
[35]T. G. Philbin and U. Leonhardt, Phys. Rev. A **78**, 042107 (2008).
[36]R. Zhao, T. Koschny, and C. M. Soukoulis, Opt. Express **18**, 14553 (2010).
[37]I. V. Lindell, A. H. Shivola, S. A. Tretyakov, and A. J. Viitanen, *Electromagnetic Waves in Chiral and Bi-Isotropic Media* (Artech House, Boston, 1994).
[38]X. J. Wang, S. Basu, and Z. M. Zhang, J. Phys. D: Appl. Phys. **42**, 245403 (2009).
[39]A. Narayanaswamy and G. Chen, Appl. Phys. Lett. **82**, 3544 (2003).
[40]D. Korobkin, Y. A. Urzhumov, B. Neuner, C. Zorman, Z. Zhang, I. D. Mayergoyz, and G. Shvets, Appl. Phys. A: Mater. Sci. Process. **88**, 605 (2007).
[41]C. Wu, B. Neuner III, J. John, A. Milder, B. Zollars, S. Savoy, and G. Shvets, J. Opt. **14**(2), 024005 (2012).
[42]A. C. Jones and M. B. Raschke, Nano Lett. **12**, 1475 (2012).
[43]S. Zhang, Y.-S. Park, J. Li, X. Lu, W. Zhang, and X. Zhang, Phys. Rev. Lett. **102**, 023901 (2009).
[44]C. Helgert, E. Pshenay-Severin, M. Falkner, C. Menzel, C. Rockstuhl, E.-B. Kley, A. Tünnermann, F. Lederer, and T. Pertsch, Nano Lett. **11**, 4400 (2011).